

# Numerical simulation of rock avalanches: Influence of a local dissipative contact model on the collective behavior of granular flows

Guilhem Mollon,<sup>1</sup> Vincent Richefeu,<sup>1</sup> Pascal Villard,<sup>1</sup> and Dominique Daudon<sup>1</sup>

Received 27 August 2011; revised 8 May 2012; accepted 11 May 2012; published 26 June 2012.

[1] Rock avalanches are a significant concern in developing mountain areas. Thus a reliable prediction of depositional areas from avalanches is needed. In order to improve the numerical modeling of such events and to provide information concerning the physical phenomena underlying this type of granular flow, a discrete element model, which takes into account frictional and collisional dissipation at grain scale together with angular-shaped elements, is used to investigate the collective behavior of granular masses propagating down a slope. The discrete element model (DEM) parameters are defined from drop tests involving the collision of an individual particle with a flat surface. The validity of the numerical model is estimated by comparison with the results of a laboratory experiment involving a dry granular flow on an inclined plane. The numerical model improves the understanding of rock avalanches by providing both valuable information about the way energy is dissipated either at the base or within the propagating granular mass and relevant information about the kinematics of the flow and the shape of the deposit. The influence of contact-law parameters is investigated using a sensitivity study. It is shown that the flow is strongly influenced by basal friction, while inter-particle friction and collisional dissipation phenomena intervene mostly in areas of flow perturbation (such as transition zones between two slopes). A macroscopic roughness of the slope surface induces an increased disorder in the particle motion which increases both frictional and collisional dissipation within the granular mass. Using a planar slope and increasing the frictional parameter can reproduce the apparent influence of this roughness.

**Citation:** Mollon, G., V. Richefeu, P. Villard, and D. Daudon (2012), Numerical simulation of rock avalanches: Influence of a local dissipative contact model on the collective behavior of granular flows, *J. Geophys. Res.*, 117, F02036, doi:10.1029/2011JF002202.

## 1. Introduction

[2] Today, the construction of housing and civil engineering infrastructure in mountain areas is on the increase. These projects are at risk from natural disasters such as rockfalls, rock avalanches, landslides, wet debris flows or snow avalanches. These risks are intensified by the effects of climate change: the increase in rainfall, storms, atmospheric warming, and rapidly alternating freeze/thaw cycles, all of which strongly destabilize rock masses. These devastating events sometimes lead to a tragic loss of life and to material damage. Rock mass movements, ranging from the fall of single blocks to several million cubic meter rock avalanches, are among the most frequent and unpredictable natural events in mountainous areas. Infrastructures (such as roads

and railways) and the populations living in these areas are particularly affected by these phenomena.

[3] To provide reliable information regarding rock avalanche related risks, a method for predicting the depositional areas of such avalanches is needed. Such predictive capability requires a better understanding of granular flow propagation.

[4] While the trajectory of individual blocks and the position of the stop zone can be approximated satisfactorily using software based on point mechanics, predicting the propagation of granular masses and the position of the deposits remains problematic. This is due to the complex collective motion of a dense flow that involves the collision of blocks, the fragmentation of blocks, and substrate erosion during flow.

[5] Several authors have studied gravity-related instability phenomena, such as trajectory-prediction of the fall of single blocks or the mass propagation of rock avalanches. Observations and analyses of real events are very complex, and many small-scale laboratory experiments [Savage and Hutter, 1991; Hutter *et al.*, 1995; Okura *et al.*, 2000a; Iverson *et al.*, 2004; Manzella and Labouse, 2008] have

<sup>1</sup>UJF-Grenoble 1, Grenoble-INP, CNRS UMR 5521, 3SR Lab, Grenoble, France.

Corresponding author: V. Richefeu, UJF-Grenoble 1, Grenoble-INP, CNRS UMR 5521, 3SR Lab, Grenoble F-38041, France.  
(vincent.richefeu@ujf-grenoble.fr)

©2012. American Geophysical Union. All Rights Reserved.  
0148-0227/12/2011JF002202

been used to examine the propagation of granular materials. The parameters most often investigated are the shape and size distribution of the particles, the basal friction, the volume of material, the fall height, and the slope angle [Davies and McSaveney, 1999; Okura et al., 2000b; Iverson et al., 2004; Friedmann et al., 2006; Goujon et al., 2007; Valentino et al., 2008; Manzella and Labiouse, 2009]. Generally, these analogue models provide relevant information about the propagation length, the deposit shape and the kinematics of the flow. Thus, they are relevant tools for the validation of numerical models. However, some physical quantities that could provide further clarification concerning the kinematics of the flow remain inaccessible owing to the difficulty of experimental measurements. Only the use of numerical models, which take into account the discrete nature of the flow, provides access to physical quantities such as the kinematics of each particle within the granular mass, the contact forces and the dissipated energy for each contact, the volume changes during the flow, and the spatial distribution of the solid fraction.

[6] Among the numerical models commonly used to describe rock avalanches are the continuum models based on the assumptions of fluid mechanics [Voellmy, 1955; Savage and Hutter, 1989; Hungr, 1995; Pouliquen and Forterre, 2002; Mangeney-Castelnau et al., 2003; McDougall and Hungr, 2004; Denlinger and Iverson, 2004; McDougall and Hungr, 2005; Pirulli et al., 2007], and the discrete models based on the equations of the motion applied to individual particles [Cundall and Strack, 1979; Okura et al., 2000b; Calvetti et al., 2000; Cleary and Prakash, 2004; Staron, 2008; Tommasi et al., 2008; Banton et al., 2009; Taboada and Estrada, 2009].

[7] One advantage of continuum models is their simplicity and speed. However, they remain relatively difficult to use as a predictive tool since their parameters (for example, the dynamic friction coefficient applied to the base of the flow, which reflects the mean energy dissipation of the flowing granular mass, the lateral stress coefficient, and the viscous intergranular parameter or turbulent term) are commonly calibrated by back-analysis [Iverson et al., 2004; Pirulli and Mangeney, 2008; Sosio et al., 2008]. Discrete element models use the laws of interaction between particles based on physical explanations, but are limited to small- to medium-scale events (between  $10^3$  and  $10^5 \text{ m}^3$ ) and restricted numbers of particles due to their computational cost.

[8] The model proposed here is based on the discrete element method. Its objective is to accurately describe the propagation of a granular mass down a slope and the mechanisms of energy dissipation occurring both at the base of the flow and within the granular mass. This interaction model is defined at the particle scale and takes into consideration the interaction laws integrating energy dissipation by collision and friction [Banton et al., 2009]. The contact laws used have a limited number of parameters (normal and tangential stiffnesses for contact elasticity, Coulomb friction and collisional coefficients for dissipation) that can be determined easily from single-collision tests. Compared with other dissipative models used in the modeling of dry rock avalanches (such as viscous contact models [Cleary and Prakash, 2004] or damping models [Calvetti et al., 2000; Tommasi et al., 2008]), the parameters of the proposed model require no exhaustive knowledge of the real physical

means of dissipation at the contact scale. The accuracy of the model is increased by using complex shaped elements. These elements are so-called spheropolyhedra that simplify the contact detection process and optimize computational times (when compared with polyhedra). The application of the model to the propagation of a granular mass down a slope highlights the main parameters driving the collective behavior of the moving mass.

[9] The proposed interaction model was validated by comparison with experimental results from Manzella and Labiouse [2009] involving a granular flow of small clay bricks on an inclined plane. This comparison focused both on the shape and size of the granular deposit after the release of the material, and the velocity of the flow front. The bricks used in these experiments have a regular shape and are the same size. The number of elements involved in the flow, and the conditions under which the experiments were carried out were fully reproduced by the numerical model. As this work was conducted within a collaborative framework (the European project, ALCOTRA-MASSA), the materials used in the experiments carried out by Manzella and Labiouse [2009] (bricks and substrate) were available to and used by the authors of this paper. This enabled an accurate determination of the contact model parameters through analysis of the trajectory of a single brick impacting a flat surface within velocity ranges similar to those observed in the experimental flow. Comparisons performed on a single rebound showed that the numerical model accurately describes the kinematics of a single particle before and after impact, and that it fully integrates the dissipative mechanisms by collision and friction.

[10] The advantage of the numerical model is that it gives access to quantities that are out of reach of experiments, such as the interaction forces between particles, the individual kinetic energies (in rotation and translation), and the processes of energy dissipation (collisions or friction, at the base or inside the flow), at any point on the slope. These data highlight the main mechanisms that govern the kinematics of the flow. In particular, the study of the energy dissipation modes enables a distinction to be made between the energy dissipated at the base of the flow and that dissipated within the granular mass. One can also deduce whether the energy is mainly dissipated by collisions or friction. Thus the main parameters of the numerical model can be highlighted and particular care taken in their determination. The introduction of an irregularity in the topography (obstacle, slope angle or macroscopic roughness) produces a change in the kinematics of the flow. An analysis of local particle velocity or energy dissipation modes leads to a precise quantification of the influence of these irregularities on the granular flow. The proposed numerical model permits an evaluation of the validity of certain common assumptions, such as the uniformity of velocities in the flow, the incompressibility of the flow mass, and the dissipation of energy by basal friction. Consequently, the discrete model proposed is a useful tool for the improvement of continuum models. Once validated on experiments performed under controlled conditions, the discrete model and the numerical process used for determining physical parameters could be applied to real events. Moreover, one can easily perform a sensitivity study in order to assess the influence of the contact parameters or to investigate the influence of the shape, the size, the number

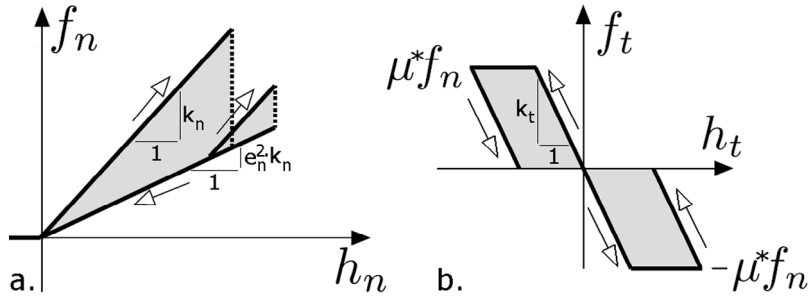


**Figure 1.** Description of the chosen interaction laws for energy dissipation during contact (in gray), with  $f_n$  and  $f_t$  (normal and tangential contact forces);  $h_n$  and  $h_t$  (normal interpenetration and tangential relative displacement);  $k_n$ ,  $k_t$ ,  $e_n^2$  and  $\mu^*$  (respectively, normal and tangential stiffnesses for contact elasticity, and collisional and tangential coefficients for dissipation): (a) force-displacement graph for normal loading and unloading; (b) force-displacement graph for tangential loading and unloading.

or the grading of the particles on the kinematics of the granular flow.

[11] First, the numerical model and the contact law used to study dissipative mechanisms at the grain scale are described in detail. Particular attention is given (Appendix A) to defining the post-processing methods needed to analyze and interpret the numerical results. Due to the discrete nature of the method used, the definition of entities such as the outline of the granular mass, the flow front velocity or the shape of the deposit, is not easy. However, precise definitions of these entities are needed to establish a satisfactory correlation with the experimental measurements.

## 2. Numerical Model

[12] A great deal of literature exists concerning the shape of elements in discrete element models [e.g., *Allen and Tildesley*, 1989; *Radjai and Dubois*, 2011]. However, in most studies the elements are assumed to be spherical for the sake of simplicity. This restriction is not a limitation in most models, because a wide range of complex behaviors can be described with great accuracy when only simple contact and friction laws are used. Specific features, such as deformability of particles [*Jerier et al.*, 2011] or “mimicry” of continuum media [e.g., *Donzé et al.*, 2009] can be obtained by introducing complex and dedicated force-laws while using rigid spheres as discrete elements. In this way, the elements can be seen as numerical points having locally averaged kinematics. Although this leads to suitable macroscopic behavior, a wide number of parameters must be carefully considered. For this reason, we approach the problem differently. Our approach involved three key steps: (1) the introduction of the dissipation processes into two “black-box” laws that address the energy balance of individual collisions regardless of the physical origins of the energy losses; (2) identifying a small number of parameters by means of single-collision-experiments; and (3) the use of realistically shaped elements. The model was implemented within the C++ toolkit DEMbox ([www.cgp-gateway.org](http://www.cgp-gateway.org)).

[13] Energy loss can result from complex physical mechanisms (heat production, wave propagation, etc.), but a simple formulation of force-laws was used here to account for energy dissipation due to collisions and friction between elements. Two laws were chosen that express the contact

force along two directions defined in a local frame: a contact force perpendicular to the contact plane,  $f_n$ , and one within the contact plane,  $f_t$ . Each force-law incorporates a coefficient of dissipation. When two elements overlap, the contact force  $f_n$  is expressed as a function of the penetration distance  $h_n$  (positive value), and its time-derivative  $\dot{h}_n$  of the touching elements as follows:

$$f_n(t + \delta t) = \begin{cases} f_n(t) + k_n \dot{h}_n \delta t & \text{if } \dot{h}_n \geq 0 \\ e_n^2 k_n h_n & \text{if } \dot{h}_n < 0 \end{cases}, \quad (1)$$

where  $\delta t$  is a small increment in time, and the parameters  $k_n$  and  $e_n^2$  correspond to the contact stiffness and the coefficient of dissipation involved in the direction perpendicular to the contact plane respectively (Figure 1a).

[14] Force  $f_t$  is incrementally updated using a strategy developed by *Hart et al.* [1988]. For simplicity, the tangential law is presented here in a simplified formalism:

$$f_t(t + \delta t) = \min\{f_t(t) + k_t \dot{h}_t \delta t ; \mu^* f_n\}, \quad (2)$$

where  $k_t$  is the tangential stiffness,  $\mu^*$  is the coefficient of tangential dissipation,  $h_t$  and  $\dot{h}_t$  are respectively the displacement and the velocity in the tangential direction (Figure 1b). It is important to understand that this coefficient can involve more than pure friction. It can translate all the mechanisms that occur in the tangential direction such as static/dynamic friction, active pressure (in the case of substantial penetration of a block into a smooth substrate), or breakage of soil particles.

[15] The advantages of the proposed interaction laws are linked to their simplicity, since the four parameters ( $k_n$ ,  $e_n^2$ ,  $k_t$  and  $\mu^*$ ) are easy to identify and have a relevant physical meaning. For example, the energy stored in the perpendicular direction during an impact is partially restored thanks to the  $e_n^2$  coefficient without any intervening residual deformation at the interface after impact. In the case of a perfect vertical fall to a horizontal plane, this coefficient (corresponding to the ratio between the unloading and loading stiffnesses) is significant, and is equal to the ratio between the drop height and the maximum height after impact.

[16] The force laws incorporate four parameters, which must be optimized by minimizing an error function based on an experimentally identified trajectory. To simplify, it is

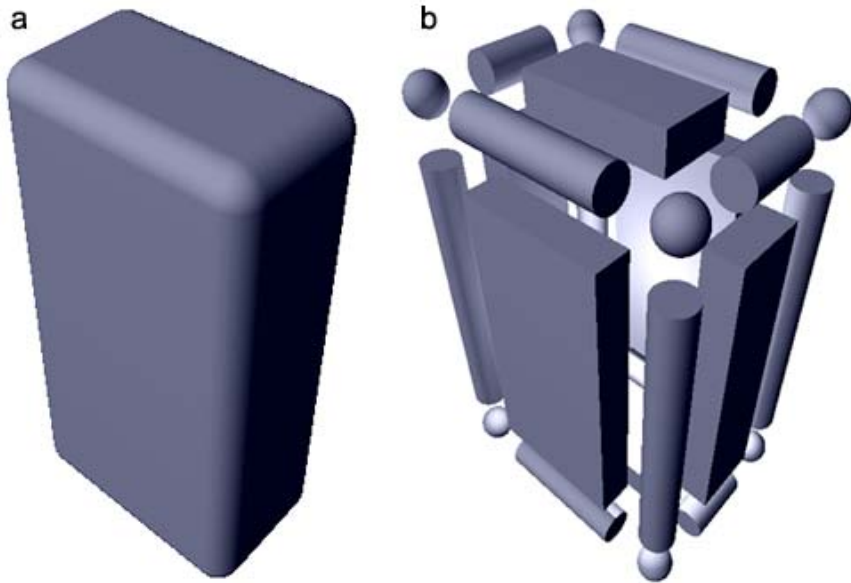


**Figure 2.** Modeling of complex block shapes by spheropolyhedra (height = 31 mm, length = 15 mm, width = 8 mm): (a) actual shape introduced in the code; (b) view of the 26 simple elements composing the shape.

assumed that, for a range of velocities, the contact parameters are always the same, independently of the position of the contact point between the two contacting bodies. This assumption may lead to inaccuracy when describing the motion of a single particle, as a slight error on each rebound might propagate with time and induce a considerable difference of trajectory after a long period of simulation. However, a slight error in the description of each rebound is irrelevant to the study of the collective behavior, especially since the parameters were averaged over a set of largely differentiated configurations of single impact (results not shown). This small inaccuracy is therefore attenuated by the large number of impacts occurring during the granular flow.

[17] The shape of the blocks is of primary importance. For example, particle shape greatly influences stress transmission throughout a granular medium and also affects volume change. Particle shape is thus taken into account explicitly in the model. Although different strategies are possible (e.g., convex polyhedra, clumps) we model each element shape as a spheropolyhedron (Figure 2), that is the shape resulting from the sweeping of a sphere onto the surface of a polyhedron. This model shape has several advantages including highly simplified contact detection [Alonso-Marroquín, 2008]. The shape of the block is defined by a set of vertices interconnected by their edges and faces (Figure 2). The rounded shape is then defined by sweeping a sphere of radius  $r$  along each of its edges and faces. In practice, the contact position, the overlap, and the local frame are determined by taking into consideration a few basic geometric computations based on the distances between points, lines and planes. This enables the contact area between spheropolyhedra to be defined by a finite set of contact points resulting from elementary intersection tests involving the swept sphere radii: (1) vertex-vertex; (2) vertex-edge; (3) edge-edge; and (4) vertex-face. One can better appreciate the benefit of this method when considering, for example, a face-face

intersection test: it is simply replaced by a set of edge-edge and vertex-face tests. The spheropolyhedra method has many other benefits such as the ability to define concave shapes. Moreover, the normal vectors at contacts are well defined.

[18] One of the advantages of the discrete approach is to provide access to energy dissipation at the contact level (that is without assuming a flow profile or using a continuum field of data). It is possible to calculate, between times  $t_0$  and  $t$ , the work  $W_N$  and  $W_T$  done by contact forces  $\alpha$  in the normal and tangential directions within a region  $\Omega$  as:

$$W_N(t_0, t) = \int_{t_0}^t \sum_{\alpha \in \Omega} f_n^\alpha \dot{h}_n^\alpha dt, \quad (3)$$

and

$$W_T(t_0, t) = \int_{t_0}^t \sum_{\alpha \in \Omega} f_t^\alpha \dot{h}_t^\alpha dt. \quad (4)$$

### 3. Calibration and Validation of the Model

#### 3.1. Description of the Reference Experiment

[19] In order to assess the predictive ability of the proposed model, an attempt was made to numerically reproduce the results of the laboratory experiment by *Manzella and Labouse* [2009]. This experiment (Figure 3), referred to hereafter as the reference experiment, consists of the launch, fall, and deposition of a granular mass along a planar slope having a sharp change of gradient. The upper slope was inclined at 45° while the lower slope was horizontal. Forty liters of small clay bricks, measuring 31 × 15 × 8 mm, were randomly dropped into a rectangular box (dimensions 0.4 ×

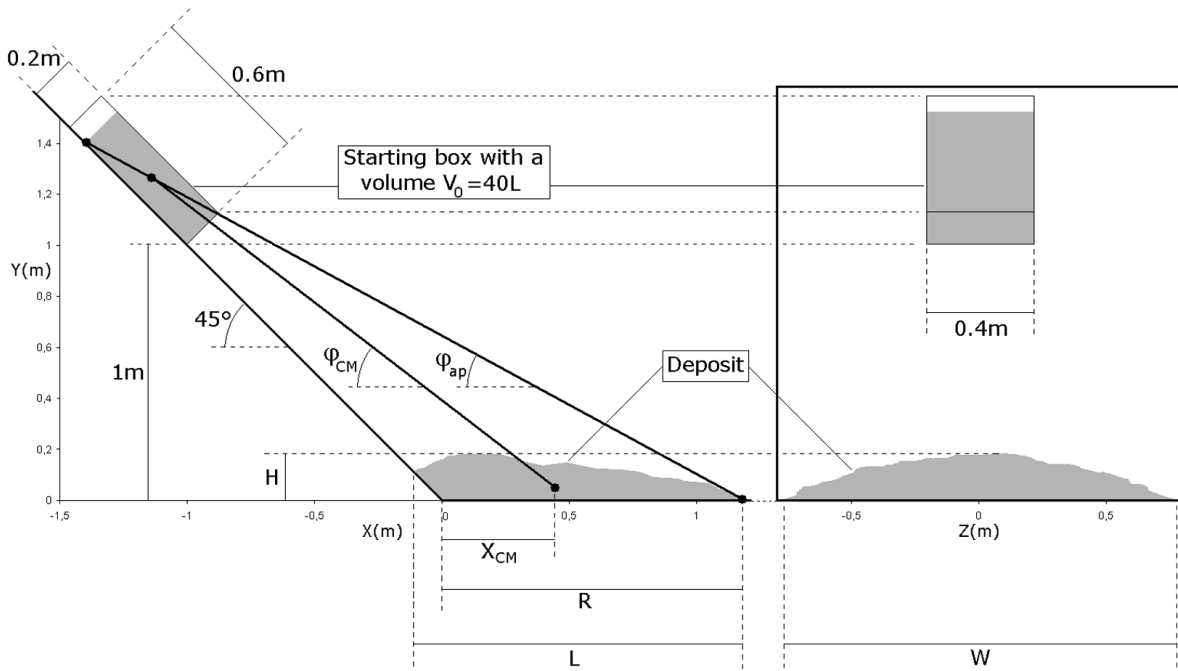


**Figure 3.** Layout of the experimental device designed by *Manzella and Labiouse* [2009], with the measured quantities  $H$  (deposit height),  $L$  (deposit length),  $R$  (deposit runout),  $W$  (deposit width),  $X_{CM}$  (X-coordinate of the center of mass),  $\varphi_{CM}$  (travel angle, with respect to the center of mass of the granular mass), and  $\varphi_{ap}$  (fahrböschung, with respect to the extreme points of the granular mass).

$0.2 \times 0.6$  m). Block density was  $1,700$  kg/m $^3$ , and the bulk density of the packed bricks was  $1,000$  kg/m $^3$ . The box was positioned at a height of  $1$  m above the inclined plane, its lower face was opened and the material was released onto the slope. The velocity of the granular mass during the flow and the dimensions of the material deposit on the horizontal plane were measured using optical methods.

### 3.2. Identification of the Parameters

[20] Back-analysis of the experimental results by *Manzella and Labiouse* [2009] would not demonstrate sufficiently rigorously the predictive character of the numerical model. Therefore, the identification of the parameters involved in the individual contact laws was scrutinized through additional experimentation. These experiments were conducted to determine the three-dimensional (3-D) trajectory of a brick before and after its collision with a flat surface made either of clay or plastic forex (i.e., the same materials used in the reference experiment). For each of these additional experiments, a single brick was dropped from diverse positions and heights. In each case, the velocity of the single brick before impact was close to the average velocity of the particles in the granular flow experiment. The fall, impact on the horizontal plane, and rebound of the brick were filmed using two high-speed cameras (1,000 frames per second). Digital image correlation was used to define the 3-D trajectory (position, rotation, velocity, and angular velocity) of the brick before and after impact. Parameters from these trajectories were then used to run a back-analysis with the numerical model. Four brick-substrate and two brick-brick impacts were carried out to describe the two types of contact occurring in a granular flow. For each of these types of

contact, the four parameters of the numerical model were optimized by minimizing an error function describing the least squared difference between the experimental and numerical trajectories as a function of the parameters  $k_n$ ,  $e_n^2$ ,  $k_t$ , and  $\mu^*$ . Table 1 shows the parameters resulting from this optimization.

[21] The values of these parameters were obtained for velocity impacts close to  $2$  m/s. A number of authors [*Tillett*, 1954; *Imre et al.*, 2008] have shown a velocity dependence of the normal restitution coefficient. This variation could be considerable for high impact speeds or for very low ones. [*Hussainova et al.*, 1999]. For the velocity range in this study, this variation was likely limited to  $10\%$  [*Imre et al.*, 2008]. By using velocity independent contact laws, the use of supplementary parameters was avoided. However, caution should be exercised when dealing with a wide range of velocities, which may be the case in natural events. This important feature has not yet been included in the present study, which focuses only on analogue experiments.

[22] Optimization of the model parameters shows that energy dissipation is more sensitive for inter-particle collisions than for brick-substrate collisions. In the latter case, due to the nature of the interactions between the clay brick

**Table 1.** Optimum Values of the Contact Parameters  $e_n^2$  and  $\mu^*$ ,  $k_n$ , and  $k_t$ <sup>a</sup>

	$e_n^2$	$\mu^*$	$k_n$ (N/m)	$k_t/k_n$
Brick-Substrate contact (BS)	0.53	0.46	100,000	0.42
Brick-Brick contact (BB)	0.13	0.86	100,000	0.27

<sup>a</sup>Respectively, collisional and tangential coefficients for dissipation, and normal and tangential stiffnesses for contact elasticity.

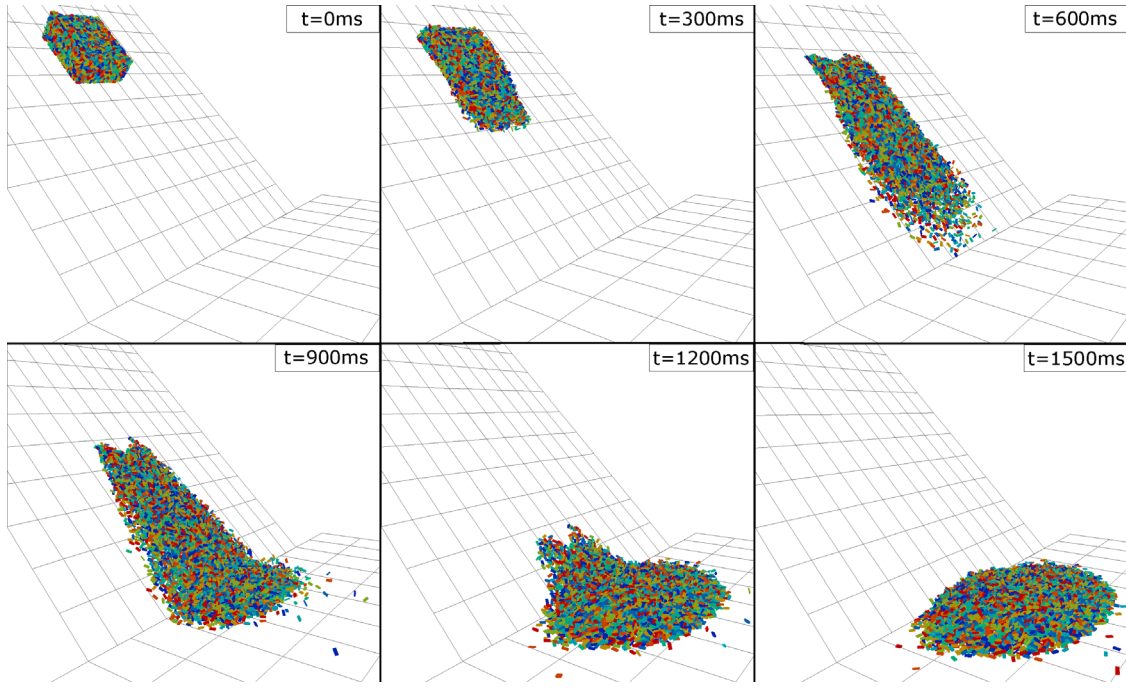


**Figure 4.** A perspective view of the numerical simulation of the reference experiment at several time steps.

and the forex substrate, the tangential energy dissipation seems to be related to friction, because the identified friction angle ( $26^\circ$  corresponding to  $\mu^* = 0.46$ ) is intermediate between measured dynamic ( $20^\circ$ ) and static ( $30^\circ$ ) friction angles provided by *Manzella and Labiouse* [2009] (using exactly the same materials). For brick-brick contact, the coefficient of tangential dissipation results partly from friction, but also from more complex energy dissipation phenomena. One can of course speculate about the physical nature of these phenomena (e.g., local hardening or micro-cracking), but we decided to simplify this critical issue by using a “black-box” law that implements a controlled energy balance using the parameter  $\mu^*$ . Moreover, it appears from Table 1 that the collisional dissipation coefficient for brick-brick contact is also much greater than that for brick-substrate contact. Our analysis also revealed that the parameters related to the contact stiffnesses in the normal and tangential directions (namely  $k_n$  and  $k_t$ ) exert only a minor influence on the particle trajectories after impact. This observation, however, proved correct only for brick-brick and brick-substrate contacts between brick and plastic forex used by *Manzella and Labiouse* [2009]. Results may differ for impacts of a rock on a soft soil. This complex issue is not accounted for in the current form of the model.

### 3.3. Validation of the Model

[23] The contact parameters were identified (by means of single collision tests) with one objective in mind: to use them in a full modeling of the experimental results obtained by *Manzella and Labiouse* [2009]. Our numerical model reproduced the geometry of the experimental device, and used 6,300 bricks modeled by spheropolyhedra. These bricks were first dropped randomly by gravity into a box. This box was then moved to its correct position on the

inclined plane, and its lower face removed at  $t = 0$  to trigger the avalanche. In all simulations performed, the value of the time increment within the model was  $5 \times 10^{-6}$  second. Figure 4 shows a perspective view of the granular flow, from release to deposition.

[24] The numerical and experimental results are compared in Figure 5. Correspondence between the numerical and experimental results was very satisfying, especially in terms of deposit geometry (Figure 5a). Good, but less satisfactory correspondence was achieved in terms of flow front velocity across the horizontal plane (Figure 5b). The small quantitative difference in velocity may be explained by the lack of precision of the concept of the front of the avalanche. The position  $X$  of this front is determined using optical techniques in the experiments, whereas its position is determined in the numerical model using a post-processing procedure. Despite this uncertainty, the numerical results (Figure 5b) appear relevant. The model gives a first description of the kinematics leading to the deposit, and shows that the motion of the avalanche on the horizontal plane may be divided into three stages: from  $X = 0$  m (corresponding to the transition line between the planes) to  $X = 0.2$  m, the avalanche velocity decreases considerably, which corresponds to the first impact of the flow on the horizontal plane. From  $X = 0.2$  m to  $X = 0.6$  m, the granular mass accumulates on the horizontal plane and its velocity decreases more slowly because of a transfer of momentum between the rear and the front of the mass, as recognized by other authors [Heim, 1932; *Van Gassen and Crueden*, 1989; Legros, 2002; *Manzella and Labiouse*, 2009]. From  $X = 0.6$  m to  $X = 0.8$  m, the velocity decreases rapidly (the same rate of deceleration as in the first stage) until the end of the motion.

[25] The satisfactory correspondence between the experimental and numerical results demonstrates the predictive

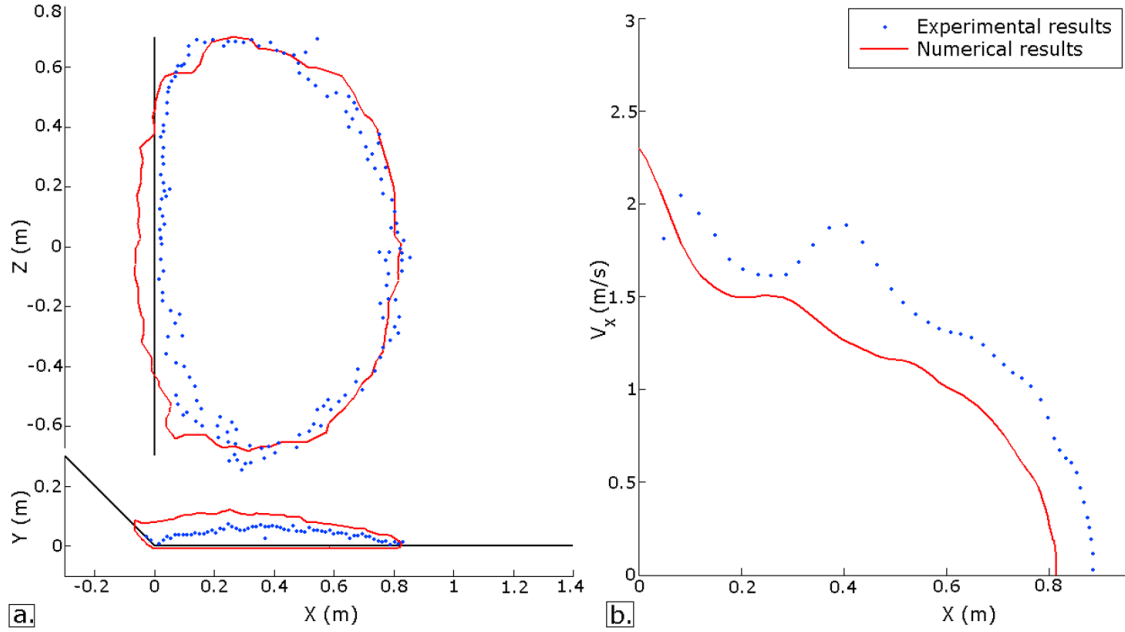


**Figure 5.** Comparison between experimental and numerical results in the reference case: (a) top-view and side-view of the contours of the deposit; (b) horizontal velocity of the front of the avalanche with respect to the position of this front on the horizontal plane ( $X = 0$  m corresponds to the transition line between the planes).

ability of the numerical model. We emphasize that physical parameters were not determined by back-analysis of the full-flow results but rather by considering single-particle impacts and then applying those results to the full particle model. The main benefit of this model is that it makes it possible to gain access to certain quantities (i.e., particle velocities and angular velocities, stress fields, flow dilation, and energy dissipations) that are unattainable in experiments.

#### 4. Analysis of the Reference Simulation

##### 4.1. Study of the Kinematics of the Event

[26] The simulation of the experiment performed by *Manzella and Labiouse* [2009] was studied closely by applying the post-processing method described in Appendix A. The simulated outline of the deposit is shown in Figure 6. The volume of this deposit is 57 L, which means that the mass dilated by a factor of 1.4 from its initial volume in the hopper. The temporal evolution of flow volume is shown in Figure 7. As brick motion differed at the front and at the rear of the initial mass, the material dilated because of its granular character. Thus, during flow down the inclined plane, the overall of the mass volume increased progressively until it reached a maximum of 1.9 times the initial volume, when the avalanche reached the gradient transition at  $t = 0.64$  s. The volume then decreased as the granular mass accumulated on the horizontal plane, and achieved its final volume when the motion stopped. It therefore appears that the flow exhibited substantial dilation during the acceleration phase, and a re-compaction during the deceleration phase. When a rock mass is initially well-structured (that is before rearrangements arise), as is often the case with natural events, dilation of the rock mass may be considerable. To properly assess the shape and location of a granular deposit, dilation

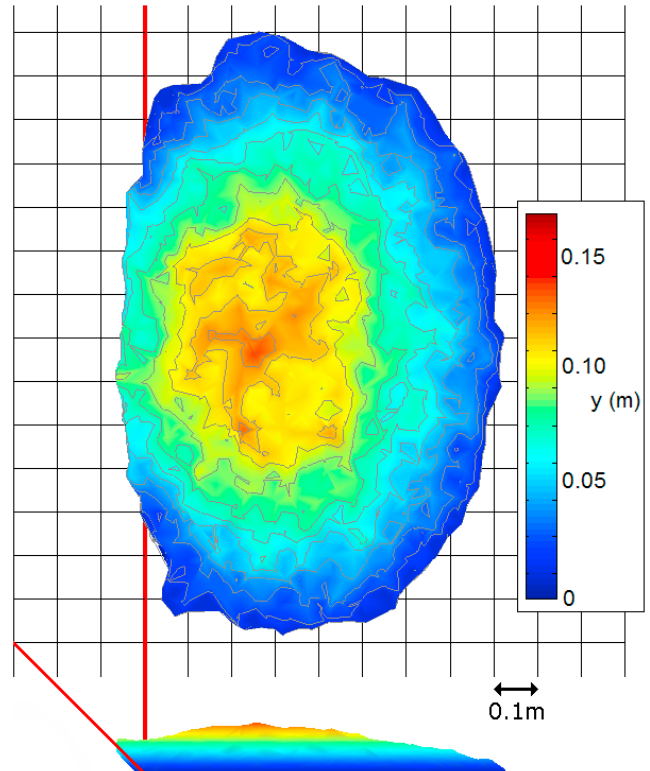


**Figure 6.** Top-view and side-view of non-convex envelope of the final deposit obtained after numerical simulation of the reference experiment (the color-scale from blue to red denotes altitude).

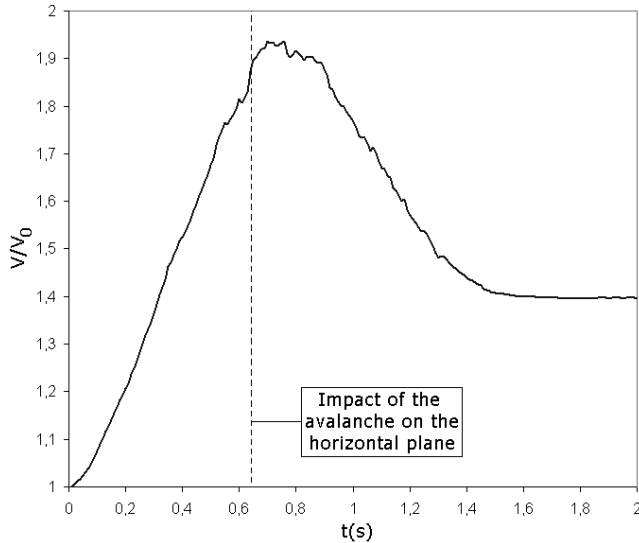


**Figure 7.** Time evolution of the relative volume  $V/V_0$  ( $V$  is the apparent volume at time  $t$  and  $V_0 = 40$  L is the initial apparent volume of the granular mass, at  $t = 0$ ) in the case of the simulation of the reference experiment.

must be considered in the numerical modeling, which is not currently the case in many models.

[27] In order to gain further insights on flow kinematic, the velocity field, the angular velocity field, and the solid-fraction field inside the flow are computed using spatial interpolation techniques. Angular velocities are considered

with respect to the instantaneous axis of rotation of each particle at a corresponding time step. This axis is different for each particle and might change during the flow, but the angular velocity of each particle about its own axis is always positive. Figure 8 demonstrates that the velocity magnitude of the particles composing the flow increases regularly as the avalanche develops, and decreases suddenly when the flow reaches the transition zone at the change in gradient. On the slope, the values of particle velocities located on the same vertical axis are very similar, showing that the flow is unaffected by horizontal shearing strains. In contrast, in the direction perpendicular to the slope, the velocity gradient is not uniform. Furthermore, the magnitude of the angular velocity of the bricks is much more substantial around the transition zone between the two planes than on the slope or in the depositional area. This is due to the change of orientation of the slope which disrupts the flow. It seems therefore that the gradient change between the two planes induces a reduction in the velocity magnitude, but also triggers a substantial perturbation of the flow by increasing particle rotation. Moreover, the angular velocity of the bricks accumulating on the horizontal plane beyond the gradient change is very low, whereas their velocity is uniform in the depositional area and decreases over time until motion ceases (at  $t = 1.4$  s). The particles in the accumulated deposit therefore exhibit a gradually decelerating translation. This motion is induced by the fact that the particles still falling down the slope transfer their kinetic energy by “pushing” the deposit beyond the gradient transition. Displacement of the accumulating deposit ends when this transfer of kinetic energy stops. This behavior correlates well with the experimental

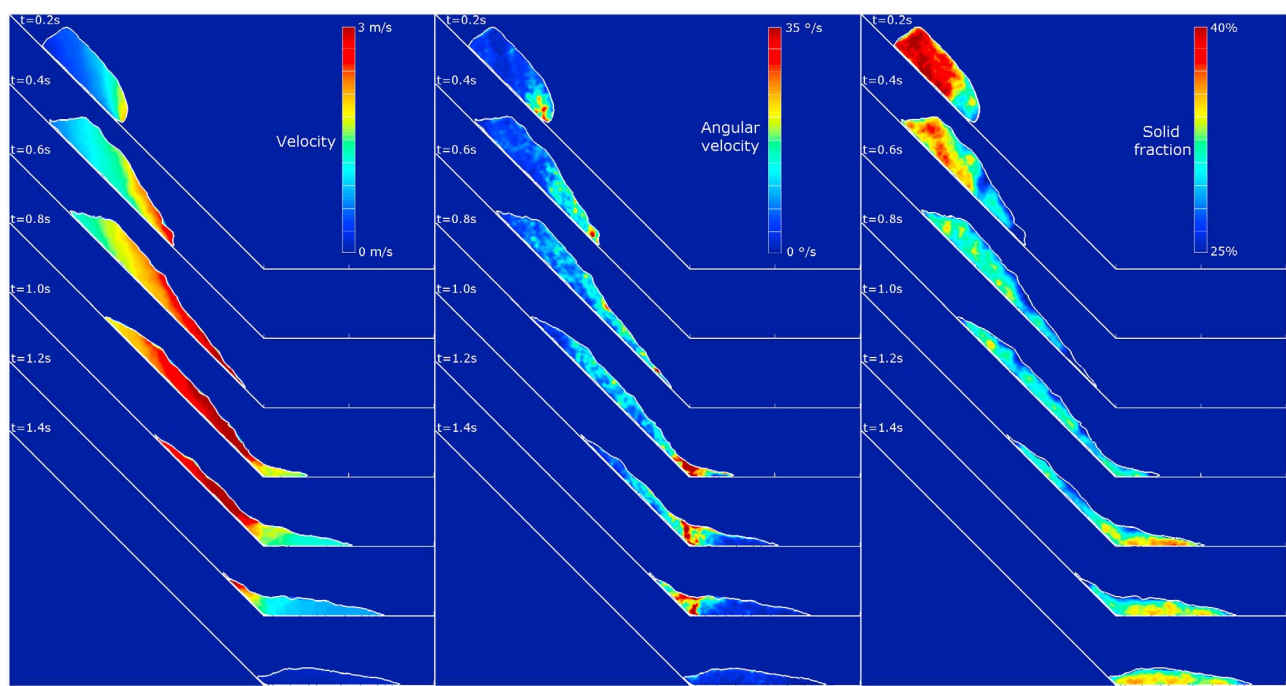


**Figure 8.** Maps of the velocity magnitude (in m/s) of the particle mass-centers, the angular velocity magnitude (in degree/s) of the particles, and the solid fraction (in %) in the plane of symmetry of the flow for the simulation of the reference experiment, at several time steps.

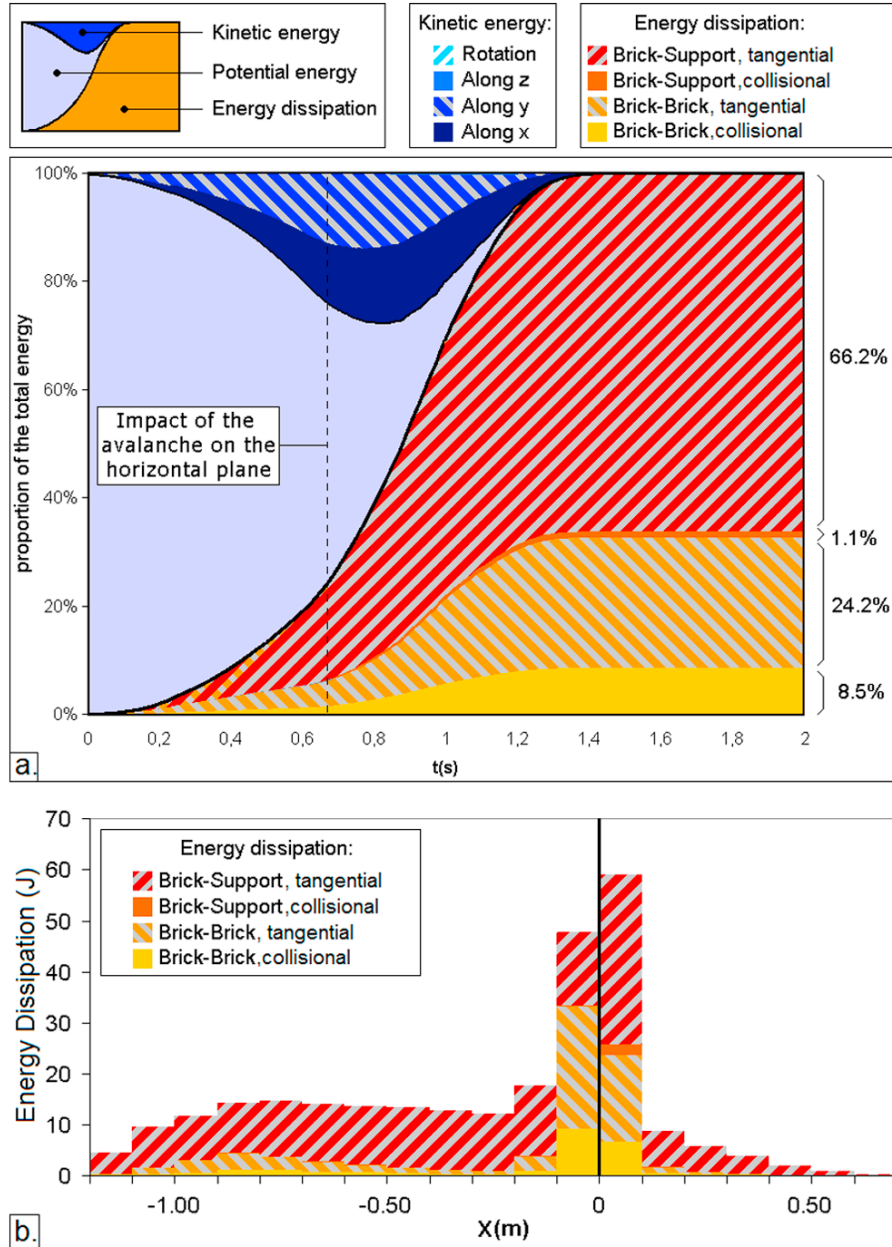


**Figure 9.** Energy transfers during the simulation of the reference experiment. (a) Time evolution of the total potential energy, total kinetic energies (along the propagation direction X, the height Y, width Z, and in rotation), and total energy dissipation (by brick-substrate friction, brick-substrate normal damping, brick-brick friction, and brick-brick normal damping). (b) Cumulated energy dissipation at the end of the flow (by brick-substrate friction, brick-substrate normal damping, brick-brick friction, and brick-brick normal damping), with respect to the X-coordinate.

and numerical estimation of flow-front velocity of the avalanche (Figure 5).

[28] The distribution of the solid fraction in the flow (Figure 8) is consistent with the dilatation and compaction observed (Figure 7). The dilation of the avalanche begins at the lower part of the granular mass, and propagates through the entire mass as the flow develops. The part of the flow in contact with the slope appears denser than the surface of the

flow, inducing a vertical density gradient. The granular mass re-compacts immediately beyond the gradient transition.

#### 4.2. Energy Considerations

[29] The analysis of the modes of energy dissipation during the flow is a useful tool to determine the relative importance of each of the parameters of the contact laws and to understand the physical mechanisms involved during the flow. As a flow evolves, different kinds of energies (potential energy,

**Table 2.** Contact Parameters  $e_n^2$  and  $\mu^*$ <sup>a</sup>

	0 (ref)	1	2	3	4	5	6	7	8
$e_n^2_{BB}$	0.13	<u>0.08</u>	<u>0.80</u>	0.13	0.13	0.13	0.13	0.13	0.13
$\mu^*_{BB}$	0.86	0.86	0.86	<u>0.30</u>	<u>0.50</u>	0.86	0.86	0.86	0.86
$e_n^2_{BS}$	0.53	0.53	0.53	<u>0.53</u>	<u>0.53</u>	<u>0.08</u>	<u>0.80</u>	0.53	0.53
$\mu^*_{BS}$	0.46	0.46	0.46	0.46	0.46	<u>0.46</u>	<u>0.46</u>	<u>0.30</u>	<u>0.60</u>

<sup>a</sup>Respectively, collisional and tangential coefficients for dissipation for the brick-brick (BB) and brick-support (BS) contacts used in the 9 simulated cases. The underlined values are the ones modified when compared with the reference case.

kinetic energy, dissipated energy) inside the system also evolve. In the static state before motion begins the system has only potential energy (Figure 9a). When the flow develops along the inclined plane (from  $t = 0$  to  $t = 0.64$  s), the potential energy decreases and the kinetic energy increases due to the velocity of the particles composing the flow. The kinetic energy may be separated into its components along the X, Y, and Z axes (respectively horizontal, vertical and lateral directions), and into rotational energy. Only the components along the X and Y directions have a significant value (Figure 9a); the energies along the Z direction (lateral spreading of the granular mass) and in rotation are negligible.

[30] The sum of the kinetic and potential energies during flow is not equal to the initial potential energy owing to energy dissipation. Various causes of energy dissipation are related to the contact laws previously described, and may be divided into four categories: brick-substrate frictional dissipation, brick-substrate collisional dissipation, brick-brick frictional dissipation, and brick-brick collisional dissipation. For a given duration  $\Delta t$ , energies dissipated by friction and by collisions are calculated using equations (3) and (4).

[31] After the impact of the avalanche on the horizontal plane, the kinetic energy reaches a peak and then decreases until motion ceases, at  $t = 1.4$  s. Meanwhile, there is an increase in the total rate of energy dissipation (i.e., the slope of the envelope of the total energy dissipation increases). This is due to the change of orientation of the slope, which disrupts the flow. The dissipated energy increases until the motion stops, which corresponds to a dissipation of 100% of the initial potential energy. The proportions of the different kinds of energy dissipated (Figure 9a) clearly show that for the geometry tested most of the energy is dissipated by friction between the substrate and the bricks (66.2%), and by friction between bricks (24.2%). Energy dissipation by collision is much less significant.

[32] The localizations of the different sources of energy dissipation are shown in Figure 9b. To plot this figure, the system was divided into several horizontal segments along the x axis, each segment having a width of 0.1 m. The energy dissipation occurring in each segment was computed during the simulation, and the figure illustrates the cumulative dissipated energies of each kind and in each segment during the entire flow. In the two planes of the system (i.e., everywhere except near the break in slope at  $X = 0$ ), the energy dissipates chiefly by friction between the bricks and the substrate (around 90% of the total energy dissipated; Figure 9b). On the inclined plane, energy dissipation is low and constant on each part of the slope. In contrast much higher levels and varied patterns of dissipation are observed at the break in

slope. The greatest dissipation is by contacts between bricks (either by friction or by collision) and results from disorder in the motion of the bricks introduced at the breaking slope as they collide with and rub against one another. The extensive proportion of brick-substrate frictional dissipation observed over the whole event (Figure 9) is due to the regularity of the slope.

## 5. Sensitivity Study

[33] The influence of variation in contact law parameters on granular flow and deposit shape was examined using a sensitivity analysis. The four dissipation parameters of contact law were changed one at a time while the others were kept constant. In addition to the parameters of the reference case, two new values for each dissipation parameter were introduced. Hence, including the parameters of the reference case, this led to the nine different cases presented in Table 2. More precisely, case 0 corresponded to the reference case, and the modified parameters were  $e_n^2_{BB}$  (cases 1 and 2),  $\mu^*_{BB}$  (cases 3 and 4),  $e_n^2_{BS}$  (cases 5 and 6), and  $\mu^*_{BS}$  (cases 7 and 8). It is important to remember that these parameters are representative of the contacts between the elements, and not of a homogenized material for which DEMs are sometimes used [e.g., Chang and Taboada, 2009]. Each of these cases was simulated for three different slope angles ( $37.5^\circ$ ,  $45^\circ$ , and  $65^\circ$ ) and for the same launch height. Results of the 27 simulations are summarized in terms of deposit run-out R (m), deposit width W (m), travel angle  $\varphi_{CM}$  ( $^\circ$ ), and fahrböschung  $\varphi_{ap}$  ( $^\circ$ ) which is related to the end of the deposit as defined by Heim [1932].

[34] The angle of the slope has a considerable influence on the travel angle and on the fahrböschung (both of them being much larger for steep slopes), but has little influence on the dimensions of the deposit, especially for gentle slopes (Figure 10). Indeed, there are only minor differences in deposit dimensions between the slope angles  $37.5^\circ$  and  $45^\circ$ , while the  $65^\circ$  slope systematically leads to slightly wider and longer deposits. The parameters related to normal damping  $e_n^2_{BB}$  and  $e_n^2_{BS}$  (cases 1, 2, 5, and 6) do not have a great influence on the deposit dimensions, and the influence of inter-particle friction  $\mu^*_{BB}$  (cases 3 and 4) is rather limited (Figure 10). However, basal friction  $\mu^*_{BS}$  (cases 7 and 8) appears to have a strong influence on the dimensions of the deposit and on both propagation angles.

[35] The observed results are probably related to the fact that the two slope segments considered in this study are perfectly planar. This leads to quite a regular, undisturbed flow for which most of the energy dissipation is related to the basal friction (Figures 8 and 9). The use of a rugged topography (perturbation magnitude of roughly grain size) will result in a change in flow kinematics. In particular, the rotation of elements is accentuated and a disorder takes place within a greater thickness of the flow. Consequently, the energy dissipated by collision and by friction within the granular mass will be greater.

[36] One may wonder, in such a case, if it is possible, by changing only the value of the basal friction angle, to introduce the same changes in the mechanisms of energy dissipation than within a granular mass falling on an irregular topography. To answer this question, a closer study of

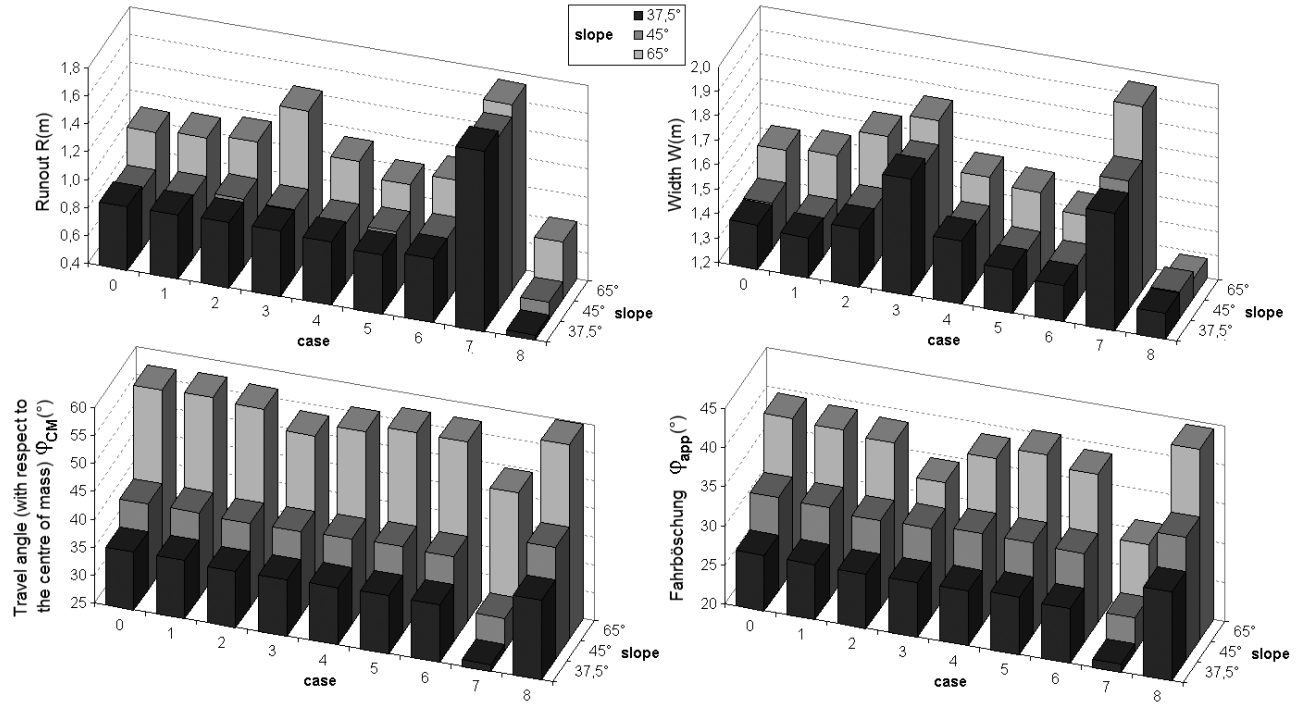


**Figure 10.** Results of the 27 simulations (9 cases including the reference case tested for 3 different slope angles) performed during the parametric study of the four dissipative parameters involved in the granular flow ( $e_{nBB}^2$ ,  $\mu_{BB}^*$ ,  $e_{nBS}^2$ , and  $\mu_{BS}^*$ ), in terms of  $R$  (deposit runout),  $W$  (deposit width),  $\varphi_{CM}$  (travel angle, with respect to the center of mass of the granular mass), and  $\varphi_{ap}$  (fahrböschung, with respect to the extreme points of the granular mass).

the influence of the basal friction on a planar or irregular slope is developed in the following section.

## 6. Influence of the Brick-Substrate Interface

[37] The inclined slope segments in the reference experiments were perfectly planar and exhibited a low coefficient of friction with the bricks ( $\mu_{BS}^* = 0.46$ ). These experimental conditions are thus quite far from those of an actual rock avalanche, because natural slopes are generally not perfectly planar and may have a much higher coefficients of friction. To obtain information about the behavior of a granular flow

under different substrate conditions, two cases are compared in this section: case A (similar to case 8) for which the coefficient of friction of the brick/substrate contact is increased from 0.46 to 0.6 compared to the reference case; case B for which this coefficient is kept at its initial value of 0.46, but the inclined plane is replaced by an undulating non-erodible surface (inclination of 45° and the undulations of the same scale as the size of the particles). The purpose of these simulations is to decide if this macro-roughness can be satisfactorily described by a simple increase in the coefficient of tangential frictional dissipation  $\mu^*$  of the brick/substrate contact. The case of an erodible slightly pronounced

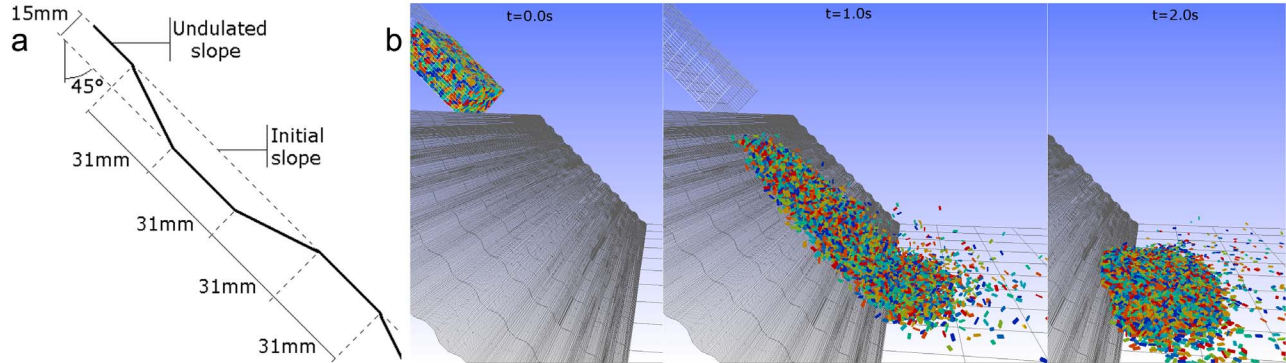


**Figure 11.** Snapshots of the flow on a slope with macro-roughness: (a) details and dimensions of the macro-roughness; (b) side-view of the flow at several times.

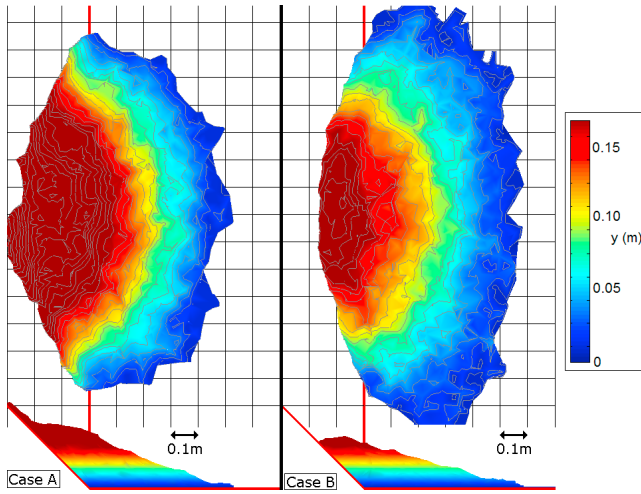


**Figure 12.** Top-view and side-view of non-convex envelopes of the final deposits obtained after numerical simulations of the flow on the smooth surface with artificially increased friction (case A) and the surface with macro-roughness (case B). The color-scale from blue to red denotes altitude.

rugosity [Taboada and Estrada, 2009] is not considered here. The coefficient of tangential frictional dissipation of 0.6 was chosen so that the deposits of cases A and B would be similar. Illustrations of the simulation of case B are provided in Figure 11. The deposits obtained at the end of the simulations of cases A and B indeed show similar behavior (Figure 12). Neither the increase in the coefficient  $\mu^*$ , nor the introduction of undulation in the slope disturbs the general organization of the deposit (Figure 13), although they do induce minor differences.

[38] When compared to the deposit of the reference simulation (Figure 6), both deposits A and B exhibit a smaller run-out and a greater thickness, because a large part of the granular mass does not reach the horizontal plane and remains on the slope. Regarding only the deposits, one may

therefore assume that a higher coefficient of friction as well as slope macro-roughness have a similar effect, and that the irregularities of a natural slope may be accounted for by a proper increase in the friction coefficient in simulations. However, the behavior of the granular mass during the flow is not the same for both cases (Figure 14). In particular, the dilation observed during the flow in case A is slightly greater than that of the reference case, and the dilation in case B is much greater than in the other two cases. Therefore slope irregularities (case B) greatly increase the volume dilation of the granular mass, whereas a simple increase of the friction coefficient (case A) is not sufficient to properly simulate this phenomenon.

[39] A simple increase in friction angle (case A) does not change the overall behavior of a flow with respect to the reference case (Figure 8). Indeed, the velocity field is very regular, and the angular velocity of the bricks remains quite low except around the break in slope. The only difference induced by the increased friction coefficient is a decrease in the magnitudes of the velocities, which reduces the “pushing” effect previously discussed, and therefore leads to a much smaller run-out. The introduction of macro-roughness (case B) on the slope, however induces a vertical velocity gradient related to shearing strain in the flow (the bricks in contact with the substrate being slower than the ones on the surface), and a greater angular velocity of the particles all along the slope related to turbulence. During the flow on the rough slope ( $t$  between 0.4 s and 1.8 s), the solid fraction of the granular mass is also lower than in case A, which correlates well with the results shown in Figures 14 and 15. These observations mean that the trajectories of the particle during flow are disturbed far more by the macroscopic roughness of the undulated slope than by an increase in the basal friction of a planar slope, although deposition is not much different in both cases. At the end of the flow, the final deposits obtained in cases A, B and the reference case, reach the same bulk density.

[40] Total energy loss, in terms of the envelopes of the total kinetic energies and of the total energy dissipation, are

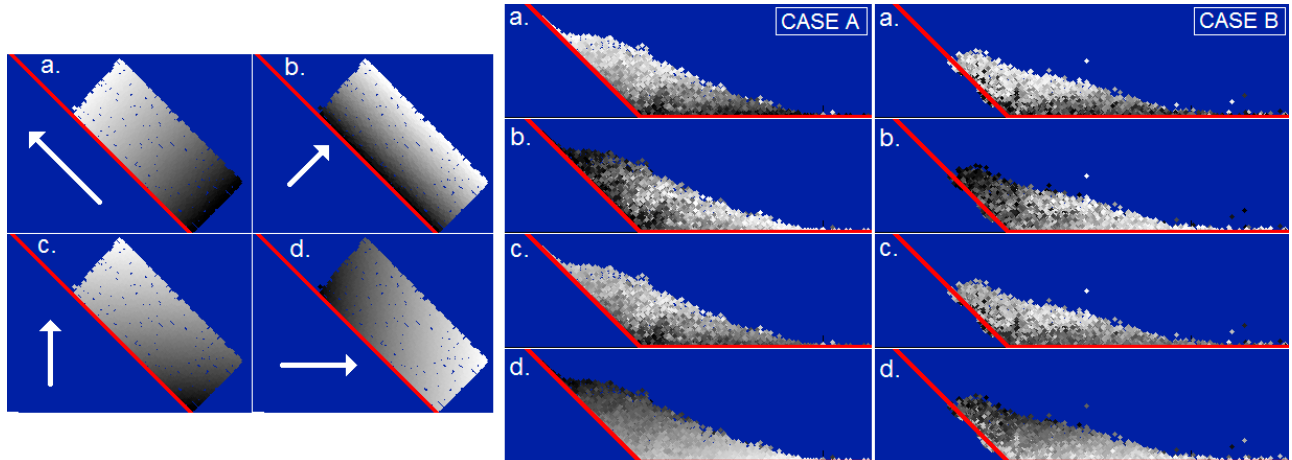


**Figure 13.** Comparison of the particle arrangement in the mass released with that in the final deposit for two simulations: the case with smooth surface and artificially increased friction (case A), and the case with surface macro-roughness (case B). (a, b, c, and d) The arrows indicate the initial layering of the gray scales with color gradient from black to white.

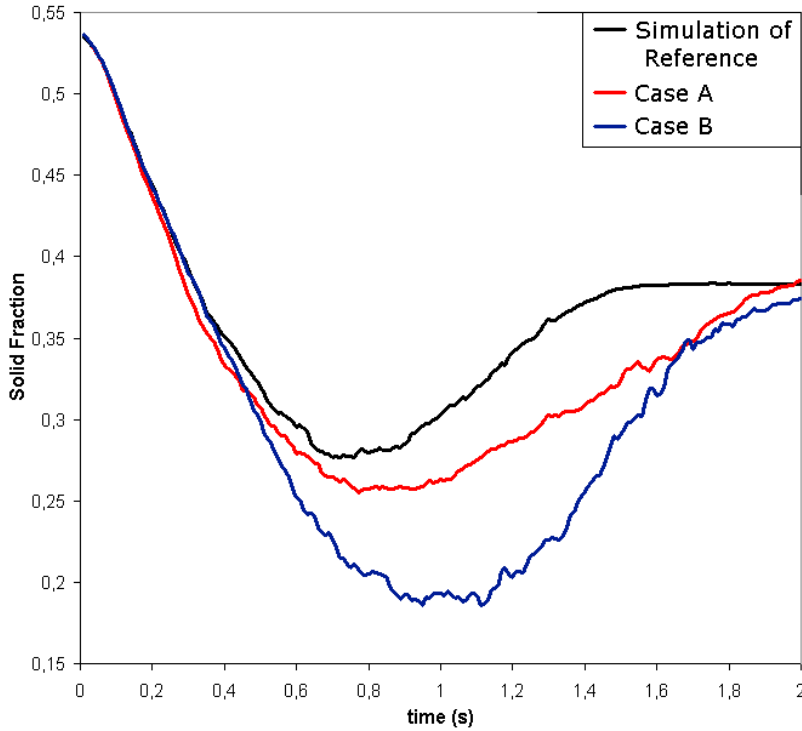


**Figure 14.** Evolution along time of the overall solid fraction of the granular mass as provided by 3 simulations: the reference case, the case with smooth surface and artificially increased friction (case A), and the case with surface macro-roughness (case B).

almost identical for macro-roughness and highly frictional smooth slopes (Figure 16a). However, the proportions of the different sources of energy dissipation differ substantially. For the high friction smooth slope simulation most of the energy is dissipated by brick-substrate friction, similar to that in the reference case (Figures 9a and 16a). In contrast, most of the energy is dissipated by brick-brick collision for the simulation of the macro-rough slope. Thus, the perturbation of flow induced by the slope undulations increases the role of inter-particle contacts in energy dissipation, because of the considerable vertical velocity gradient that is introduced (Figure 16b). Thus, all the phenomena which only occurred near the break in slope in the reference case can occur anywhere on an irregular slope provided that the flow can be sufficiently perturbed from regularity. These phenomena cannot be observed by simply increasing the coefficient of friction on the slope.

## 7. Conclusion

[41] To study dry granular mass flow, a discrete element model was developed. Our model focused on the shapes of the elements and the appropriate contact laws that account for energy dissipation due to collisions occurring in the direction perpendicular to the contact plane and to friction in the tangential direction. The parameters of the contact model were identified from experiments involving a series of impacts between two blocks or between a single block and a substrate. By optimizing the parameters for each contact, the numerical model described accurately the collective motion of the elements on a slope.

[42] Using realistic geometries for the blocks and the substrate, and characterizing the balance of energy loss at the contact level, the discrete element method adequately modeled an experimental granular flow by *Manzella and Labiouse* [2009]. However, because of the limited number of elements, the numerical model is best suited to natural events that involve small or medium-sized volumes – in general those less than  $10^5 \text{ m}^3$ . Conversely, continuum models such as those adopting shallow layer approaches, cannot handle these particular cases because they involve a small number of blocks and the assumption of a continuous kinematic field become too much strong.

[43] Numerical analysis of the spatial and temporal distribution of the type of energy loss during the flow showed that basal friction on a smooth planar slope had the greatest influence on the amount of energy dissipated during flow, whereas interactions between the blocks predominated when obstacles or irregular topography perturbed the flow.

[44] The numerical model also highlighted depositional aspects of rock avalanches. As slope gradient declines the front of the avalanche is deposited, then the tail of the flow pushes the initial deposit, thus increasing the run-out and leading to the common deposit morphology. Such a depositional process for granular flows has been described previously [e.g., *Heim*, 1932; *Van Gassen and Crueden*, 1989; *Legros*, 2002].

[45] Our numerical analysis showed that assumptions of uniformly distributed velocity in a vertical cross section and energy dissipation by basal friction are valid for dry granular flows on a smooth planar slope. However, these assumptions

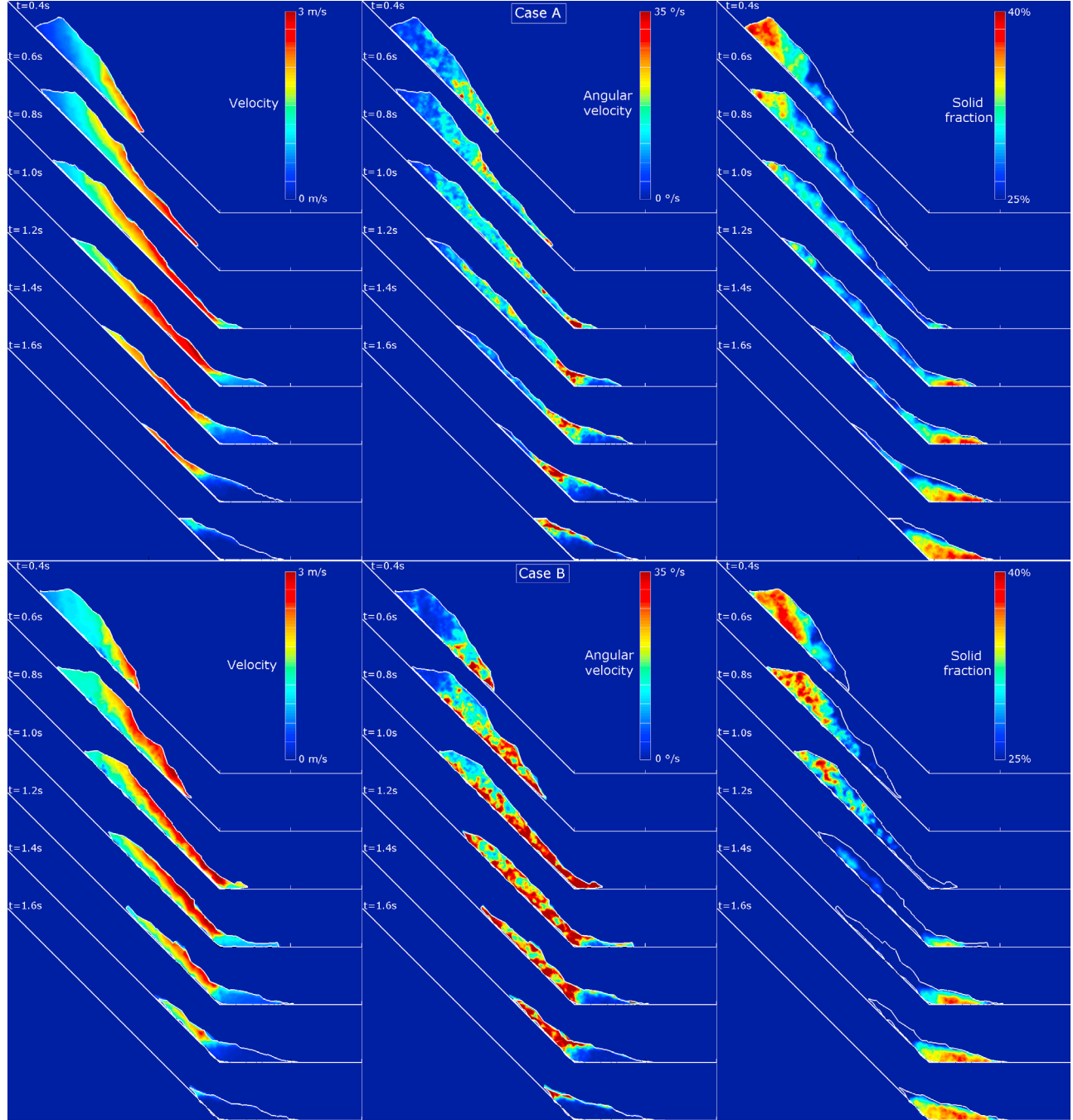


**Figure 15.** Maps at several time steps of the mass center velocities of the particles, the angular velocities of the particles, and the solid fraction in the plane of symmetry of the flow for 2 cases: smooth surface with artificially increased friction (case A), and surface macro-roughness (case B).

are not valid when flow is perturbed by an abrupt change in gradient to a shallow slope.

[46] The influence of the topography (whether irregular or smooth) on flow is significant. Surface irregularities significantly change the nature of a flow and the way energy is dissipated. Flow across an irregular surface is more easily perturbed, which promotes dissipation by collision and friction between particles. Increasing the tangential friction coefficient between particles and a substrate is a way to introduce this effect when a model uses a smooth surface.

[47] To develop fuller potential, our proposed model needs to be tested in more experiments and on natural rock avalanches. Its main asset is that it implements a limited number of parameters which are easily assessable.

[48] At present, our model is well suited to small-scale events, and can be a useful tool in providing relevant information about the kinematics of granular flows, but it can be improved by taking into account more complex dissipative phenomena (e.g., velocity dependence of energy loss after a collision). To take into account phenomena such as deep

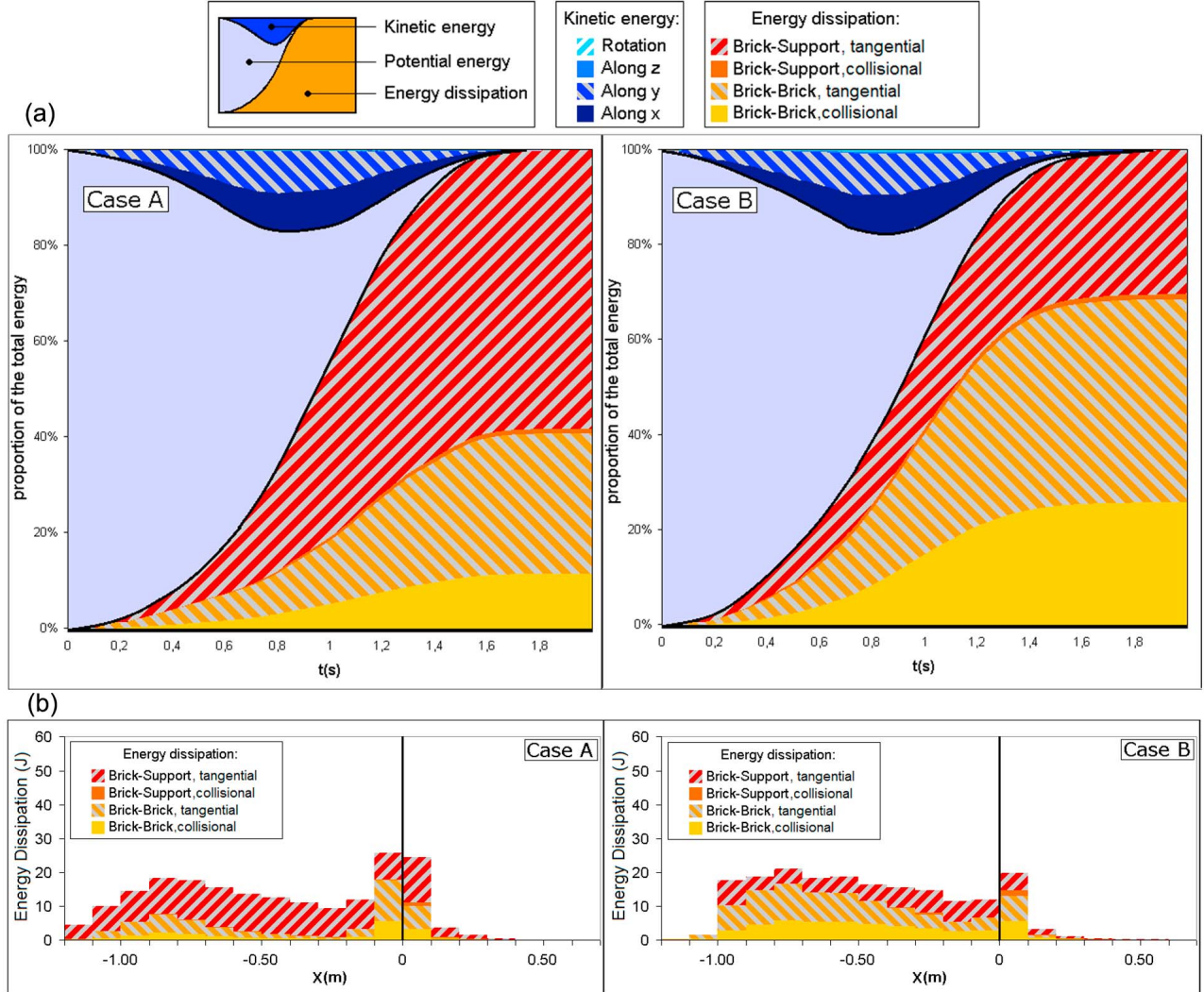


**Figure 16.** Comparison of the energy transfers between 2 cases: smooth surface with artificially increased friction (case A), and surface macro-roughness (case B): (a) time evolution of the total potential energy, total kinetic energies (along the propagation direction X, the height Y, width Z, and in rotation), and total energy dissipation (by brick-substrate friction, brick-substrate normal damping, brick-brick friction, and brick-brick normal damping), (b) cumulated energy dissipation at the end of the flow (by brick-substrate friction, brick-substrate normal damping, brick-brick friction, and brick-brick normal damping), with respect to the X-coordinate.

penetration of a block into soft soil, or the fracturing of blocks, contact laws need to be improved. Although implementation of such laws in a discrete element code is feasible, the main difficulty is in the determination of the additional parameters.

## Appendix A: Numerical Methods of Post-Processing

[49] The DEM model provides at each step a list of the  $N_0$  particles with their coordinates ( $x, y, z$ ), rotations ( $r_x, r_y, r_z$ ), velocities ( $v_x, v_y, v_z$ ), and angular velocities ( $\omega_x, \omega_y, \omega_z$ ). It also provides a list of the forces applied to each particle (including the magnitude, direction, and point of application of these forces). This substantial amount of data requires

several steps of post-processing in order to extract the relevant information about the granular flow.

### A1. Estimation of the Position of the Front and Tail of the Avalanche

[50] A correct assessment of the kinematics of an avalanche requires knowledge of the position of its back end and front end limits over time, respectively denoted  $X_{\min}(t)$  and  $X_{\max}(t)$ . Since the cloud of particles is in a disordered state during the flow, no absolute method exists for an accurate determination of the intuitive limits of the avalanche. A simple method is proposed hereafter. First, the irrelevant particles are removed from the avalanche, i.e., the ones which apparently do not belong to the main flow because their trajectory separated them from the others. These particles are detected quite

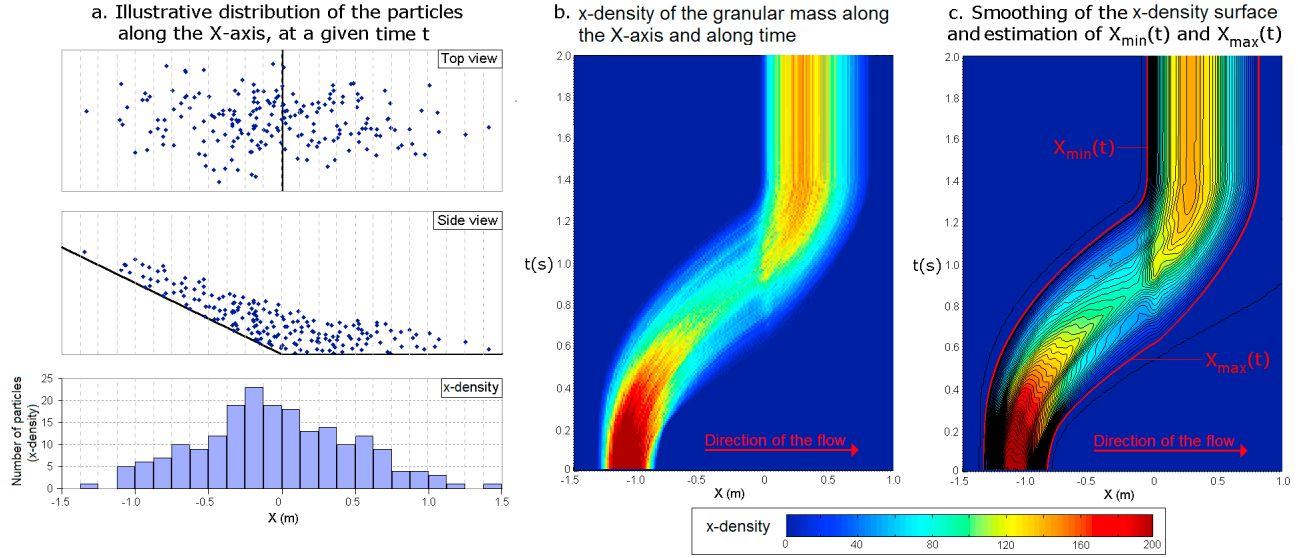


**Figure A1.** Steps of post-processing for the assessment of the position of the avalanche front: (a) determination of the particle distribution along the  $x$  axis in an illustrative case; (b) raw distribution of the particles along the  $x$  axis and along time in the case of the simulation of the reference experiment; (c) smoothing of the surface in the  $(X, t)$  plane obtained from Figure A1b and estimation of the position of the front and rear limits (respectively  $X_{\max}(t)$  and  $X_{\min}(t)$ ) of the granular flow at each time step.

easily (based on the condition that there is no other particle around them within a distance of 30 mm, i.e., roughly the length of a brick), and are evicted from the numerical process so that the avalanche can be defined by a single “dense” cloud of particles. It should be emphasized that a given particle may leave the main avalanche at the beginning of the flow but rejoin it later, depending on its trajectory. All the particles are therefore tested at each time step, and a number  $N_1(t)$  of particles are retained whereas a number  $N_0-N_1(t)$  are disregarded.

[s1] Even when these particles are removed from the avalanche, its limits are difficult to assess. For example, if the first and last particles of the flow are considered the limits of the avalanche this leads to irrelevant results along the flow because the velocity of the avalanche as a whole is different from the velocity of its individual, extreme particles. To be relevant, the limits of the flow should be assessed by a clear, reproducible method and be consistent with the “intuitive limits” of the granular mass. They should also evolve steadily during the flow.

[s2] Two functions are therefore sought,  $X_{\min}(t)$  and  $X_{\max}(t)$ , representing the positions of the rear and front limits of the flow on the  $x$  axis. In order to define these functions, the flow is divided into a considerable number of segments, each of a constant length along the  $x$  axis. In each segment  $j$ , at a time step  $t$ , there are a given number of particles. This number of particles will hereafter be called the “ $x$ -density” of the flow, and can be considered a 1D projection of the flow on the  $x$  axis. Figure A1a presents the way to compute the  $x$ -density at a given time step  $t$ , for an illustrative case. A simple way to assess the “ $x$ -extremities” of the granular mass is to choose the values  $X_{\min}$  and  $X_{\max}$  for which the  $x$ -density disappears below a prescribed threshold. Figure A1b provides a top view of the same data for the reference simulation of this study, at all the time steps of the simulation.

This chart is therefore plotted in an  $(x, t)$  frame. However, it is still very difficult to assess the position of extremities  $X_{\min}(t)$  and  $X_{\max}(t)$  of the avalanche from this figure due to the irregularity of the  $x$ -density surface obtained. Hence, a smoothing (using the classical LOWESS algorithm already implemented in MATLAB) of the surface is carried out, see Figure A1c. The choice of the  $x$ -density threshold must be made carefully. It should neither be too low (otherwise the  $x$ -extremities of the granular mass might be disturbed by a few particles which leave the main flow) nor too high (otherwise the estimated  $x$ -extremities of the flow may exclude a very large number of particles). The best value for the threshold is highly problem-dependent, so it is advisable to proceed by trial and error: the threshold value should be fixed as low as possible, provided that it does not lead to  $x$ -extremities visually diverging from the main flow because of a few isolated particles. In the present problem, a value of 5 was found to be suitable. The level contour curves corresponding to this  $x$ -density threshold (in red) are plotted in Figure A1c, and appear to be very smooth over time. These curves therefore approximate the extremities  $X_{\min}(t)$  and  $X_{\max}(t)$  of the avalanche. The regularity of  $X_{\min}(t)$  and  $X_{\max}(t)$  arising from this method makes it possible to obtain a correct, smooth estimation of the velocities of the tail and front of the avalanche (by simple numerical derivation of  $X_{\min}(t)$  and  $X_{\max}(t)$ ), which would not have been possible otherwise.

## A2. Definition of the Non-convex Envelope of the Avalanche

[s3] The convex hull of a cloud of points is unique and may be determined using a large number of well-known algorithms. However, such an envelope gives little information on the spatial distribution of the points inside the cloud. In the

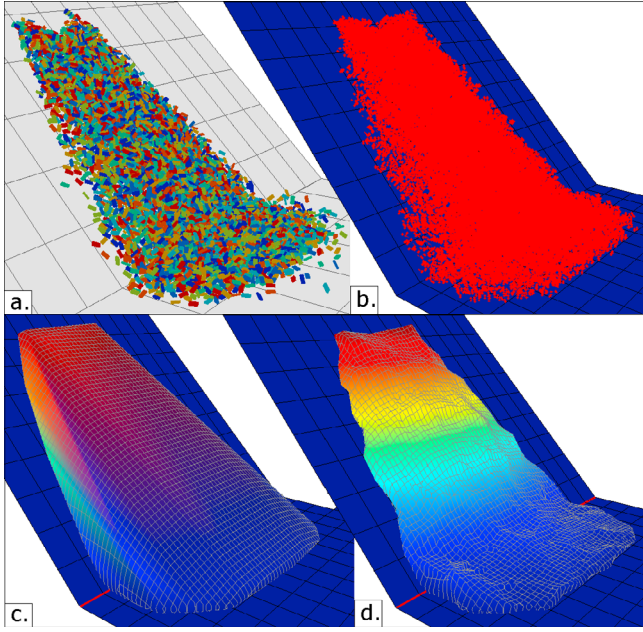


**Figure A2.** Determination of the non-convex envelope of the flow: (a) raw result from the DEM simulation (position and orientation of each particle); (b) cloud of points composed by the eight corners of each brick; (c) convex envelope of this cloud of points (corresponding to  $\alpha = +\infty$  in the  $\alpha$ -shape algorithm); (d) non-convex envelope of this cloud of points (corresponding to  $\alpha = 0.05$  m).

case of a granular avalanche, the flow may have a strongly non-convex shape because of the possible irregularities of the topography. The use of a convex envelope would lead to the necessity to account for large empty volumes inside the convex contour of the cloud of points, and would prevent an accurate estimation of the solid fraction of the granular mass. It is therefore necessary to define a more precise non-convex hull, although such a hull is well-known to be non-unique. *Edelsbrunner et al.* [1983] proposed a method based on the so-called “ $\alpha$ -shapes” to determine the non-convex hull of a 2D set of points, and *Edelsbrunner and Mücke* [1994] extended this to 3D. This method defines a non-convex hull depending on a single parameter  $\alpha$ . First, the cloud of points is submitted to a Delaunay triangulation, i.e., the convex hull of the cloud of points is divided into a collection of tetrahedrons. Then, the principle of the  $\alpha$ -shapes method consists in retaining only the tetrahedrons respecting the condition  $R_c < \alpha$ ,  $R_c$  being the radius of their circumscribed spheres. The union of the remaining tetrahedrons forms a region of space which is unique for a given  $\alpha$  and provides an intuitive non-convex envelope of the considered cloud of points. Note that for  $\alpha = +\infty$  this method provides the exact convex hull of the cloud [*Edelsbrunner and Mücke*, 1994].

[54] In the case of the brick-avalanche considered in the present study, the cloud of points is composed at a time  $t$ , of the eight corners of each of the bricks. Figure A2 presents the successive steps of the method. Figure A2a shows the direct result of the numerical model in an illustrative case, Figure A2b shows the cloud of points (corresponding to the

8 corners of each brick) introduced in the  $\alpha$ -shape algorithm, and Figures A2c and A2d show the envelopes provided by the algorithm for  $\alpha = +\infty$  (convex envelope) and  $\alpha = 0.05$  m. As can be seen in Figure A2, the value  $\alpha = 0.05$  m leads to visually satisfying non-convex envelopes of the flow. In the general case, the value of  $\alpha$  should be chosen in such a way that: (i) the contour of the region defined by the  $\alpha$ -shapes is as close as possible to the “real” contour of the discrete particles (for this purpose,  $\alpha$  should be as low as possible), and (ii) the region defined by the  $\alpha$ -shapes is not composed of several disjointed regions but is rather one whole region (for this purpose,  $\alpha$  should not be too low). This second point has of course to be fulfilled only if the granular flow is actually considered “one mass” (though there is no absolute definition for this term). In general, it is advisable to use a value of  $\alpha$  close to twice the largest dimension of the largest particle of the flow. With such a value, the region defined by the alpha-shapes will closely wrap the assembly of the discrete particles without separating the flow into disjointed regions. In our case, the value  $\alpha = 5$  cm is consistent with the size of the bricks (3.1 cm in length) but it should be noted however that the best choice of  $\alpha$  is highly problem-dependent.

[55] This step makes the computation of the total volume of the avalanche (defined as the sum of the volumes of the tetrahedrons composing the non-convex hull) possible. Moreover it has the advantage of defining the notions of “inside” and “outside” of the flow (i.e., a given point of the space is located inside the flow if it belongs to one of the tetrahedrons of the non-convex hull, otherwise it is outside).

### A3. Solid Fraction

[56] The understanding of flow kinematics requires a study of the local density of the granular mass (defined by the solid fraction). This parameter is difficult to assess because it requires the study of a sufficiently substantial amount of particles in order for it to have a meaning at the point scale. A method of assessment of the solid fraction related to each particle is proposed hereafter, although the determination of this parameter in a granular flow is not unique.

[57] First, a representative volume is defined for the particle around which the solid fraction is needed. This representative volume is defined by the non-convex envelope (as defined in the previous subsection) of the cloud of points composed of the eight corners of the particle and its  $n_v$  closest neighbors. The total representative volume  $V_{tot}$  is computed from the non-convex envelope, and the volume  $V_m$  of material inside  $V_{tot}$  is defined by the volume of the particles. The solid fraction attached to the spatial coordinates of the particle is then given by:

$$s = V_m / V_{tot} \quad (A1)$$

A number  $n_v = 50$  shows satisfying results and is chosen for the following steps. This number is higher than the numbers of particles which are commonly used to define a representative volume for the study of granular materials (between 15 and 30), because of a possible flaw in the computation of  $s$ . Indeed, the proposed method does not account for some particles the center of mass of which may be located outside the representative volume but which may intersect with its

surface. Some matter inside the representative volume may thus be unaccounted for and the local solid fraction may be underestimated by this method. The use of a non-convex envelope which closely “wraps” the  $n_v$  particles limits this drawback. This inaccuracy is also reduced when one increases the number of particles inside the representative volume, which is the reason why the number of 50 particles was chosen. The authors believe that this method, despite its minor drawback, provides a good qualitative assessment of the density distribution inside the flow.

#### A4. Interpolation of Particle-Attached Scalars

[58] The graphical analysis of scalar fields might provide more information about the physics of the flow. Those fields are difficult to plot because the considered scalars are attached to the spatial coordinates of each particle and not positioned on a regular grid. This is, for example, the case of the velocity magnitudes of the particles in the flow. However, from the concept of  $\alpha$ -shapes, it is possible to access equivalent continuous fields of particle-related scalars using a simple interpolation technique. The non-convex hull of the avalanche is first defined using the concept of  $\alpha$ -shapes but considering the center of mass of each particle (instead of its eight corners, as was the case in the previous subsection, in order to be able to interpolate between the centers of the particles). This non-convex hull is therefore defined as a collection of tetrahedrons, and each of these tetrahedrons defines the region of space lying between the centers of four particles of the flow (corresponding to the four vertices of the tetrahedron considered).

[59] For any point in space, it is then very easy (though computationally expensive) to assess if it belongs to the non-convex hull and, if so, to which tetrahedron in particular. The value of the scalar field at this point is then obtained directly by linear interpolation between the values of this scalar property at the four corners of the tetrahedron. If this operation is performed for each point of a regular grid, it makes it possible to plot an equivalent scalar field of the considered property. One should note however that such a continuous field has no physical existence (the considered scalars being attached to discrete particles) and should only be considered a useful tool to observe qualitatively some phenomena occurring in the flow.

[60] **Acknowledgment.** This research project was carried out within the framework of the European project, ALCOTRA-MASSA, with financial support from the *European Funds For Regional Development* (FEDER).

#### References

- Allen, M. P., and D. J. Tildesley (1989), *Computer Simulation of Liquids*, Clarendon Press, New York.
- Alonso-Marroquín, F. (2008), Spheropolygons: A new method to simulate conservative and dissipative interactions between 2d complex-shaped rigid bodies, *Europhys. Lett.*, 83(1), 14001, doi:10.1209/0295-5075/83/14001.
- Banton, J., P. Villard, D. Jongmans, and C. Scavia (2009), Two-dimensional discrete element models of debris avalanches: Parameterization and the reproducibility of experimental results, *J. Geophys. Res.*, 114, F04013, doi:10.1029/2008JF001161.
- Calvetti, F., G. B. Crosta, and M. Tarella (2000), Numerical simulation of dry granular flows: From the reproduction of small-scale experiments to the prediction of rock avalanches, *Rivista Ital. Geotecnica*, 2, 21–38.
- Chang, K. J., and A. Taboada (2009), Discrete element simulation of the Jiufengershan rock-and-soil avalanche triggered by the 1999 Chi-Chi earthquake, Taiwan, *J. Geophys. Res.*, 114, F03003, doi:10.1029/2008JF001075.
- Cleary, P. W., and M. Prakash (2004), Discrete-element modeling and smoothed particle hydrodynamics: Potential in the environmental sciences, *Philos. Trans. R. Soc. London, Ser. A*, 362, 2003–2030, doi:10.1098/rsta.2004.1428.
- Cundall, P. A., and O. D. L. Strack (1979), A discrete numerical-model for granular assemblies, *Geotechnique*, 29(1), 47–65, doi:10.1680/geot.1979.29.1.47.
- Davies, T. R., and M. J. McSaveney (1999), Runout of dry granular avalanches, *Can. Geotech. J.*, 36, 313–320, doi:10.1139/t98-108.
- Denlinger, R. P., and R. M. Iverson (2004), Granular avalanches across irregular three-dimensional terrain: 1. Theory and computation, *J. Geophys. Res.*, 109, F01014, doi:10.1029/2003JF000085.
- Donzé, F. V., V. Richet, and S. A. Magnier (2009), Advances in discrete element method applied to soil, rock and concrete mechanics, *Electr. J. Geotech. Eng.*, 13, 1–44.
- Edelsbrunner, H., and E. P. Mücke (1994), Three-dimensional alpha shapes, *ACM Trans. Graphics*, 13, 43–72, doi:0730-0301/94/0100-0042.
- Edelsbrunner, H., D. G. Kirkpatrick, and R. Seidel (1983), On the shape of a set of points in the plane, *IEEE Trans. Inf. Theory*, 29, 551–559, doi:10.1109/TIT.1983.1056714.
- Friedmann, S. J., N. Taberlet, and W. Losert (2006), Rock-avalanche dynamics: Insights from granular physics experiments, *Int. J. Earth Sci.*, 95, 911–919, doi:10.1007/s00531-006-0067-9.
- Goujon, C., B. Dalloz-Dubruleaud, and N. Thomas (2007), Bidisperse granular avalanches on inclined planes: A rich variety of behaviors, *Eur. Phys. J. E*, 23, 199–215, doi:10.1140/epje/i2006-10175-0.
- Hart, R., P. Cundall, and J. Lemos (1988), Formulation of a three-dimensional distinct element model—part II: Mechanical calculations for motion and interaction of a system composed of many polyhedral blocks, *Int. J. Mech. Min. Sci. Geomech. Abstr.*, 25, 117–125, doi:10.1016/0148-9062(88)92294-2.
- Heim, A. (1932), *Bergsturz und Menschenleben*, 218 pp., Fretz und Wasmuth Verlag, Zürich.
- Hungr, O. (1995), A model for the runout analysis of rapid flow slides, debris flows, and avalanches, *Can. Geotech. J.*, 32(4), 610–623, doi:10.1139/v95-063.
- Hussainova, I., J. Kübarsepp, and I. Shcheglov (1999), Investigation of impact of solid particles against hard metal and cermet targets, *Tribol. Int.*, 32, 337–344, doi:10.1016/S0301-679X(99)00073-0.
- Hutter, K., T. Koch, C. Plüss, and S. B. Savage (1995), The dynamics of avalanches of granular-materials from initiation to runout. 2. Experiments, *Acta Mech.*, 109, 127–165, doi:10.1007/BF01176820.
- Imre, B., S. Rabasen, and S. M. Springman (2008), A coefficient of restitution of rock materials, *Comput. Geosci.*, 34, 339–350, doi:10.1016/j.cageo.2007.04.004.
- Iverson, R. M., M. Logan, and R. P. Denlinger (2004), Granular avalanches across irregular three-dimensional terrain: 2. Experimental tests, *J. Geophys. Res.*, 109, F01015, doi:10.1029/2003JF000084.
- Jerier, J. F., G. Hathong, V. Richet, B. Chareyre, D. Imbault, F. V. Donze, and P. Doremus (2011), Study of cold powder compaction by using the discrete element method, *Powder Technol.*, 208(2), 537–541, doi:10.1016/j.powtec.2010.08.056.
- Legros, F. (2002), The mobility of long-runout landslides, *Eng. Geol. Amsterdam*, 63, 301–331, doi:10.1016/S0013-7952(01)00090-4.
- Mangeney-Castelnau, A., J. P. Vilotte, M. O. Bristeau, B. Perthame, F. Bouchut, C. Simeoni, and S. Yerneni (2003), Numerical modeling of avalanches based on Saint-Venant equations using a kinetic scheme, *J. Geophys. Res.*, 108(B11), 2527, doi:10.1029/2002JB002024.
- Manzella, I., and V. Labiouse (2008), Qualitative analysis of rock avalanches propagation by means of physical modeling of non-constrained gravel flows, *Rock Mech. Rock Eng.*, 41, 133–151, doi:10.1007/s00603-007-0134-y.
- Manzella, I., and V. Labiouse (2009), Flow experiments with gravel and blocks at small scale to investigate parameters and mechanisms involved in rock avalanches, *Eng. Geol. Amsterdam*, 109, 146–158, doi:10.1016/j.jengeo.2008.11.006.
- McDougall, S., and O. Hungr (2004), A model for the analysis of rapid landslide motion across three-dimensional terrain, *Can. Geotech. J.*, 41, 1084–1097, doi:10.1139/t04-052.
- McDougall, S., and O. Hungr (2005), Dynamic modelling of entrainment in rapid landslides, *Can. Geotech. J.*, 42, 1437–1448, doi:10.1139/t05-064.
- Okura, Y., H. Kitahara, T. Sammori, and A. Kawanami (2000a), The effects of rockfall volume on runout distance, *Eng. Geol. Amsterdam*, 58, 109–124, doi:10.1016/S0013-7952(00)00049-1.
- Okura, Y., H. Kitahara, and T. Sammori (2000b), Fluidization in dry landslides, *Eng. Geol. Amsterdam*, 56, 347–360, doi:10.1016/S0013-7952(99)00118-0.

- Pirulli, M., and A. Mangeney (2008), Results of back-analysis of the propagation of rock avalanches as a function of the assumed rheology, *Rock Mech. Rock Eng.*, **41**(1), 59–84, doi:10.1007/s00603-007-0143-x.
- Pirulli, M., M. O. Bristea, A. Mangeney, and C. Scavia (2007), The effect of the earth pressure coefficients on the runout of granular material, *Environ. Model. Softw.*, **22**, 1437–1454, doi:10.1016/j.envsoft.2006.06.006.
- Pouliquen, O., and Y. Forterre (2002), Friction law for dense granular flows: Application to the motion of a mass down a rough inclined plane, *J. Fluid Mech.*, **453**, 133–151, doi:10.1017/S0022112001006796.
- Radjai, F., and F. Dubois (eds.) (2011), *Discrete-Element Modeling of Granular Materials*, Wiley, Hoboken, N. J.
- Savage, S. B., and K. Hutter (1989), The motion of a finite mass of granular material down a rough incline, *J. Fluid Mech.*, **199**, 177–215, doi:10.1017/S0022112089000340.
- Savage, S. B., and K. Hutter (1991), The dynamics of avalanches of granular materials from initiation to runout. 1. Analysis, *Acta Mech.*, **86**, 201–223, doi:10.1007/BF01175958.
- Sosio, R., G. B. Crosta, and O. Hungr (2008), Complete dynamic modeling calibration for the Thurwieser rock avalanche (Italian Central Alps), *Eng. Geol. Amsterdam*, **100**, 11–26, doi:10.1016/j.enggeo.2008.02.012.
- Staron, L. (2008), Mobility of long-runout rock flows: A discrete numerical investigation, *Geophys. J. Int.*, **172**, 455–463, doi:10.1111/j.1365-246X.2007.03631.x.
- Taboada, A., and N. Estrada (2009), Rock-and-soil avalanches: Theory and simulation, *J. Geophys. Res.*, **114**, F03004, doi:10.1029/2008JF001072.
- Tillett, J. P. A. (1954), A study of the impact on spheres of plates, *Proc. Phys. Soc. London, Sect. B*, **67**, 677, doi:10.1088/0370-1301/67/9/304.
- Tommasi, P., P. Campedel, C. Consorti, and R. Ribacchi (2008), A discontinuum approach to the numerical modelling of rock avalanches, *Rock Mech. Rock Eng.*, **41**(1), 37–58, doi:10.1007/s00603-007-0133-z.
- Valentino, R., G. Barla, and L. Montrasio (2008), Experimental analysis and micromechanical modelling of dry granular flow and impacts in laboratory flume tests, *Rock Mech. Rock Eng.*, **41**, 153–177, doi:10.1007/s00603-006-0126-3.
- Van Gassen, W., and D. M. Cruden (1989), Momentum transfer and friction in the debris of rock avalanches, *Can. Geotech. J.*, **26**, 623–628, doi:10.1139/t89-075.
- Voellmy, A. (1955), Über die Zerstörungskraft von Lawinen, *Schweiz. Bauztg.*, **73**, 212–285.